Low-energy electron-impact ionization of helium

E. Schow,[1] K. Hazlett,[1] J. G. Childers,[1] C. Medina,[1,*] G. Vitug,[1,†] I. Bray,[2] D. V. Fursa,[2] and M. A. Khakoo[1]
[1]*Department of Physics, California State University, Fullerton, California 92834, USA*
[2]*Centre for Atomic, Molecular and Surface Physics, School of Mathematical and Physical Sciences, Murdoch University, Perth 6150, Australia*
(Received 7 August 2005; revised manuscript received 3 October 2005; published 27 December 2005)

Normalized doubly differential cross sections for the electron-impact ionization of helium at low energies are presented. The data are taken at the incident electron energies of 26.3, 28.3, 30.3, 32.5, 34.3, 36.5, and 40.7 eV and for scattering angles of 10°–130°. The measurements involve the use of the moveable target method developed at California State University Fullerton to accurately determine the continuum background in the energy-loss spectra. Normalization of experimental data is made on a relative scale to well-established experimental differential cross sections for excitation of the $n=2$ manifold of helium and then on an absolute scale to the well-established total ionization cross sections of Shah *et al.* [J. Phys. B **21**, 2751 (1988)]. Comparisons are made with available experimental data and the results of the convergent close-coupling theory.

DOI: 10.1103/PhysRevA.72.062717 PACS number(s): 34.80.Dp, 25.30.Dh

I. INTRODUCTION

Helium has been a popular target for electron scattering studies, including pioneering studies of fundamental electron scattering processes, e.g., elastic [1] and inelastic [2] scattering, resonant scattering [3], electron-photon coincidence [4], and ionization [5]. Helium is frequently used as a calibration standard in experimental electron collision studies, since it is an inert gas that is easily handled in vacuum systems. Accurate elastic and inelastic differential cross sections (DCSs) for electron scattering from helium exist due to the considerable effort on the part of both theory and experiment. In the past decade, the convergent close-coupling (CCC) method has been applied with great success to the calculation of electron-impact excitation of atomic helium (see Fursa and Bray [6], Bray *et al.* [7], Fursa and Bray [8], and Röder *et al.* [9]). The CCC method has also been applied to the calculation of electron-impact ionization of helium (Röder *et al.* [10] and Bray and Fursa [11]). Generally, the agreement with experiments here is excellent considering the difficulty in both the theory and experiment. However, some discrepancies remain between experimentally determined doubly differential cross sections (DDCS) and the results of the CCC theory at the lower energies.

Very recently, two additional models, namely the time-dependent close-coupling theory (TDCC) of Pindzola *et al.* [12] and the exterior complex scaling model (ECS) of Horner *et al.* [13], have been applied to electron-helium scattering. However, as yet we are unaware of the ECS and TDCC approaches being applied to calculate electron-helium differential ionization cross sections. We note here that the CCC and ECS methods have been successful in modeling the electron impact of atomic hydrogen, and excellent agreement between theory and experiment over a wide range of conditions has been observed (see, e.g., Childers *et al.* [14]).

Triply differential ionization cross-section measurements (TDCS) have been carried out by the Kaiserslautern group of Ehrhardt and co-workers [15–19] for the ionization of helium at a range of incident energies (E_0). Jones *et al.* [20], using the distorted wave Born approximation, showed some agreement with the equal energy-sharing TDCSs even for near-threshold ionization. The distorted partial wave method of Pan and Starace [21] yields TDCSs only for the geometry of back-to-back outgoing electrons. This approach gives excellent agreement with such experimental TDCS taken at E_0 values of 32.6, 44.6, 64.6, and 104.6 eV [19]. Most recently, the CCC method has been applied extensively to e-He ionization and was found to give excellent quantitative agreement with experiment for all incident energies and geometries considered (Stelbovics *et al.* [22]).

There have been several measurements of doubly differential ionization cross sections (DDCSs) for the electron-impact ionization of helium. Pichou *et al.* measured near-threshold DDCSs for helium at incident energies of 25.4, 26.0, 27.0, 28.2, and 30.6 eV for scattering angle (θ) values of 10°–110°. The DDCSs of Pichou *et al.* were normalized to the elastic electron scattering differential cross sections of helium from Andrick and Bitsch [25] using the helium ionization continuum symmetry properties [i.e., flatness of the continuum energy-loss spectrum for residual energies (E_R) between 0.2 and 0.7 eV for an incident energy of 25.38 eV] to correct for their spectrometer transmission, extending the measurements piecewise to higher E_R values using higher E_0 settings. Background determinations in the Pichou *et al.* experiments were accomplished by an ad hoc method of constructing a linear background joining the baseline between the $n=3$ and 4 energy-loss features and extrapolating it to the end of the ionization continuum. This method has been shown in the present set of experiments to be unreliable; it yields systematically higher DDCSs by including unresolved

*Present address: Department of Physics, Cleveland State University, Cleveland, OH 44115, USA.
†Present address: Department of Physics, University of California, Riverside, CA 92521, USA.

secondary electron backgrounds. The extensive DDCSs of Röder *et al.* [24] were taken at E_0 values of 28.6, 32.6, 40, 50, 64.6, 100, and 200 eV and scattering angles of 20°–145°. Their data were relatively normalized (via measurement of the total helium ion current in the experiment) to the total ionization cross sections of Shah *et al.* [26] and then absolutely normalized to the $E_0=100$ eV DDCSs of the CCC theory [27]. However, there remain significant disagreements between the most recent CCC results [28], Röder *et al.* [24], and Pichou *et al.* [23]. For example, at 32.6 eV, Röder *et al.* observe good qualitative agreement between their DDCS angular distributions and those of CCC, but there are consistent quantitative disagreements between their results and CCC. The near-threshold energy region is important in that the outgoing electrons experience large correlations in this energy regime as they slowly recede from the core He^+ ion. Also, low-energy electron collisions are important in plasma environments such as planetary atmosphere physics and man-made industrial plasmas including microelectronics and lighting.

Additionally, for reference, DDCSs taken at $E_0 > 40$ eV (outside the range of this work) have been measured in the past by Opal *et al.* (100–2000 eV [29]), Oda (500 eV [30]), Rudd and Dubois (100 and 200 eV [31]), Shyn and Sharp (50, 100, 200, and 300 eV [32]), Müller-Fiedler *et al.* (100, 200, 300, 400, 500, and 600 eV [33]), and Rösel *et al.* (100, 200, 300, 400, 500, and 600 eV [34]). Based on the need for reliable quantitative low-energy electron-impact DDCSs for helium, we have measured new DDCSs for helium at E_0 values of 26.3, 28.3, 30.3, 32.5, 34.3, 36.5, and 40.7 eV. Our measurements are compared to the corresponding DDCSs of the CCC theory and available experiments.

II. METHODS

A. Experiment

The present measurements were carried out on two instruments, both of which have been discussed in previous publications. The first was equipped with a double hemisphere electron monochromator and double hemisphere electron analyzer that normally operates with an energy resolution of 40 meV or below, but was operated at a degraded resolution of 100 meV with a current of 100–120 nA (by opening the central slit between the hemispheres from 1 mm width to 2.5 mm and raising the sphere pass voltages from typically 2 to 5 eV). This instrument has been described in our recent experiments with argon and molecular nitrogen (see Khakoo *et al.* [35] and Khakoo *et al.* [36]) and was used for initial measurements at $E_0=26$ and 28 eV. The second spectrometer was a single hemisphere device in both the monochromator and the analyzer, but the system was equipped with a microwave discharge atomic hydrogen source. This apparatus has been described in Childers *et al.* [37,38]. This spectrometer operated with a current of 50–100 nA with a resolution of $\approx$140 meV. In both systems, the electron beam crossed an effusive source of gas emitted by a capillary needle source of diameter ranging from 0.5 to 0.8 mm. Surfaces surrounding the collision region (including the needle) were heavily sooted with an acetylene flame to suppress the production of secondary electrons by the primary electron beam colliding with these surfaces. In both spectrometers, the depth of field of the detector was restricted to a small region around the collision center (5–6 mm region) by using an additional pupil in the input electron lens stack of the detector. Both spectrometers were baked to greater than 120 °C to maintain stability of the electron beam and the detector. Both instruments were housed in double mu-metal shields to reduce the ambient magnetic field at the collision region to below 5 mG.

Both systems were equipped with a moveable gas target source [39]. Using the moveable source, it is possible to obtain background-free electron-energy-loss spectra for both discrete and continuum features. To ensure that the movable source did not affect the electron beam, the tip of the needle was kept at least 4 mm away from the center of the collision region, and variations of the transmitted electron beam were monitored, using an electron collecting plate arranged downstream of the collision region, as the needle was moved into and out of alignment with the incident electron beam. No variations were observed when the electron beam was placed (by spectrometer deflection plates) at the collision region center. At small scattering angles, we observed an additional source of secondary electrons possibly due to the electron beam slightly changing size (due to space-charge neutralization) at the collision region when the gas beam was moved into and out of alignment. This effect produced an additional source of secondary electrons from the analyzer shielding plates (for E_R below 1 eV) that could not be systematically removed by subtracting the electron-energy-loss spectra with the gas in and out of alignment with the incident electron beam. This added an additional 15% uncertainty to the signal for these low E_R electrons.

We calibrated the transmission of our analyzer as follows. First, the detector transmission was made as uniform as possible for electrons with different E_R values by tuning the analyzer and monitoring the flatness of the helium continuum at $E_0 \approx 30$ eV. The fact that the helium continuum energy-loss spectrum is flat was established by Pichou *et al.* [23], and was used successfully in previous work by our group in atomic hydrogen [14]. At larger E_R, this transmission was found to be stable during the course of measurements as long as the analyzer was not retuned. However, closer to zero E_R this uniform transmission could not be achieved. Accounting for the analyzer transmission at small E_R values was found to be the most difficult problem in this experiment, resulting in increased error bars at these small E_R values. We recalibrated the overall transmission as follows: Atomic hydrogen spectra were obtained (using our microwave source) in the manner described in Childers *et al.* [38] and the background-free atomic hydrogen continuum energy-loss spectrum was normalized to the exterior complex scaling (ECS) theory [40,41], which was previously established as accurate by the experimental work of Childers *et al.* [38]. By way of obtaining background-free atomic hydrogen spectra, we also obtained discharge-off background-free molecular hydrogen spectra in the same way as [38]. These H_2 spectra were calibrated for transmission using the transmission obtained from the atomic hydrogen spectra at the same E_0 and θ from the ECS theory. This transmission-corrected H_2 spectrum was used to calibrate the helium energy-loss spectrum by a relative flow method [42], where both He and H_2 were passed through the capillary with approximately the same mean free path (i.e., at drive pressures inversely proportional to the square of their molecular diameters, 2.18×10^{-8} cm for helium and 2.74×10^{-8} cm for H_2; see Rugamas *et al.* [43]), so that the collision region geometry did not affect the transmission. These calibrations were undertaken at $E_0=30$ eV for $\theta=60°$ and 90° and for $E_0=40$ eV for $\theta=50°$ and 90°. However, the best reproducibility for this calibration was obtained for the full ionization continuum at $E_0=30$ eV for $\theta=90°$, which was adopted as our most accurate determination of the transmission calibration (to approximately 8% on a relative scale), and for $E_R>10$ eV at $E_0=40$ eV, which is more than half of the continuum at this incident energy. Using the above calibrations, we were able to accurately correct for the transmission of our detector. Finally, the spectrometer transmission was extrapolated into the He ($n=2$) energy-loss region using a polynomial of order $\leqslant 2$, to enable us to normalize the energy-loss spectrum to the electron impact DCS for excitation of the He ($n=2$) energy-loss feature in our electron-energy-loss spectra.

In general, many electron-energy-loss spectra of helium were taken (usually at least three spectra per initial value of E_0 and θ, and in some cases up to 10, especially for the $\theta=90°$ spectra, which were used to check the instrumental transmission) spanning the energy-loss range of 19 eV to E_0+1 eV and covering the $n=2$ features. Sample helium energy-loss spectra showing the moveable source background removal method are shown in Figs. 1(a) and 1(b). The $\theta=90°$ spectra taken at $E_0=30$ eV served to determine the transmission characteristics of the analyzer using the H-source calibrations discussed above and these calibrations were used to recalibrate spectra taken at other angles during the same electron beam and gas beam conditions. To determine the continuum DDCS from a given energy-loss spectrum, we normalized the transmission-corrected spectrum [extrapolated into the He ($n=2$) energy-loss region via a polynomial of order $\leqslant 2$] to the experimental He ($n=2$) DCSs (summed DCSs for the electron-impact excitation of the $1\,^1S\rightarrow 2\,^3S$, $2\,^1S$, $2\,^3P$, and $2\,^1P$ transitions) measured by Hall *et al.* [42], Asmis and Allan [44], Larsen and Khakoo [45], Röder *et al.* [46], Cartwright *et al.* [47], and Cubric *et al.* [48], which were in excellent agreement in most cases to within 15% and with a conservative average standard deviation of 12%. For incident energies not covered in the previous He ($n=2$) DCS measurements, the DCS data were interpolated. The interpolated values agreed well with the CCC He ($n=2$) DCSs at lower θ values, but deviated from the CCC by as much as 16% for θ close to 130° at E_0 values near 30 eV. These helium ($n=2$) DCSs are given in Table I. Our DDCS were obtained from the transmission-corrected energy-loss spectra by the formula

$$\frac{d^2\sigma(E_0,E,\theta)}{d\Omega dE}=\frac{N(E,\text{continuum})}{N(\text{He},n=2)\Delta E}\frac{d\sigma(E_0,E,\theta)}{d\Omega}, \quad (1)$$

where $N(E$, continuum) is the height of the continuum (number of electron scattering events) at the position E (energy-loss) in the continuum, ΔE (typically set to ≈ 0.0217 and 0.0407 eV for the double hemispherical and single hemispherical setups, respectively) is the energy step width per channel in the energy-loss spectrum, $N(\text{He},n=2)$ is the total number of electron scattering events under the He ($n=2$) energy-loss features, and $d\sigma/d\Omega$ is the He ($n=2$) DCS from Table I. The value of N (E,continuum) was determined by fitting the continuum to a polynomial series in E of order $\leqslant 2$. The calibration of the spectrum was dependent upon an accurate determination of the value of ΔE. This value was determined from the energy-loss spectra in which the start energy-loss and end energy-loss values were recorded. The location of the helium $2\,^3S$ feature in the spectrum at 19.814 eV energy-loss served to calibrate E for the whole spectrum. The linearity of the energy-loss scale ramp voltage supply was determined in a separate experiment and was found to be $\approx 0.2\%$ of the energy-loss covered in the full energy-loss spectrum. The incident energy of the electron beam was determined from the spectrum by using the cutoff energy-loss value (see Fig. 1) of the continuum. This method served to determine E_0 to an accuracy of ±0.12 eV. The

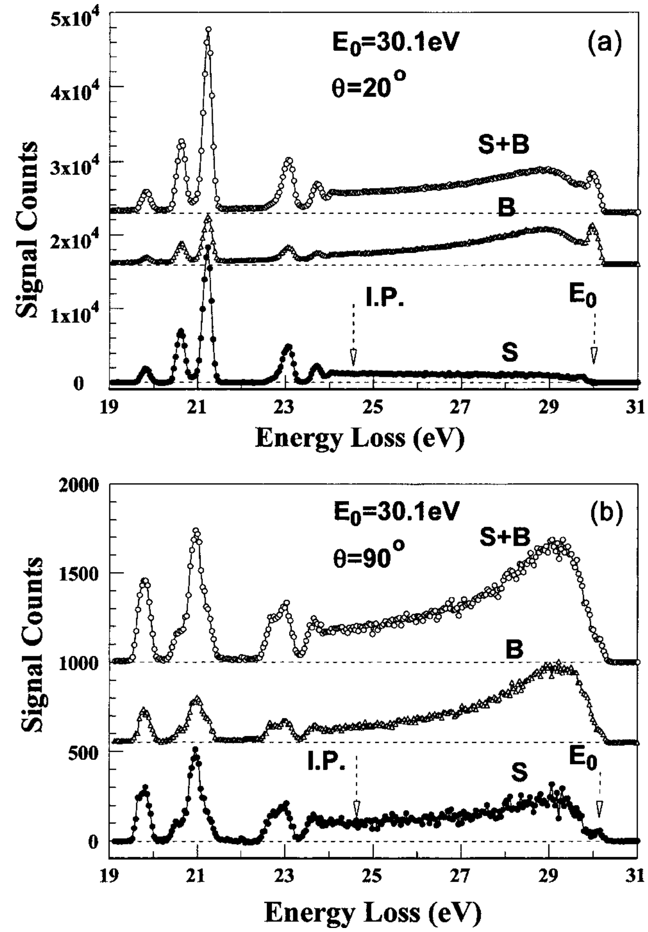

FIG. 1. Electron-energy-loss spectrum of helium at $E_0=30.1$ eV and θ of 20° and 90°. Legend:—○—Gas in (signal+background);—△—, gas out (background);—●—, gas in minus gas out (signal). The ionization potential (I.P.) and the position of E_0 (cutoff of spectra) are indicated by a vertical arrow. See text for discussion.

TABLE I. DCSs for the summed excitation of the $n=2$ levels of helium used in this work. Uncertainties for DCSs at E_0 of 22, 24, 30, and 40 eV are ±12% (one standard deviation). For other E_0 values (26, 28, 32, 34, and 36 eV), which were interpolated from the above E_0 values using the CCC as a guide, the uncertainties are ±15%. Units are in 10^{-19} cm^2 sr^{-1}. See text for discussion.

E_0 (eV)/θ (deg)	22	24	26	28	30	32	34	36	40
5	6.67	19.1	32.0	47.0	65.0	80.0	100	125	174
10	6.63	18.5	28.5	41.8	55.0	69.7	85.0	101	136
20	5.61	13.6	21.5	28.5	34.9	39.5	43.0	46.3	49.6
25	5.03	11.0	16.3	20.7	24.4	27.0	29.0	30.0	30
30	4.46	8.55	11.9	14.7	16.9	18.6	19.5	20.0	19.1
40	3.40	4.85	6.48	7.7	8.64	9.20	9.50	9.57	8.81
50	3.53	3.80	4.40	5.18	6.09	6.80	6.50	6.30	5.77
60	4.23	4.10	4.28	4.70	5.22	5.65	4.97	4.86	4.37
70	5.16	5.47	5.50	5.30	4.98	4.57	4.20	3.84	3.68
80	6.00	6.35	6.30	6.05	5.56	5.00	4.40	3.85	3.38
90	6.53	6.88	6.80	6.40	5.81	5.10	4.40	3.84	3.51
100	7.00	7.18	7.00	6.60	6.04	5.40	4.73	4.15	3.70
110	6.85	7.28	7.28	6.93	6.37	5.65	5.03	4.40	3.87
120	6.38	7.20	7.45	7.32	6.85	6.21	5.47	4.80	4.15
125	6.00	7.35	7.85	7.68	7.09	6.20	5.50	5.20	4.25
130	5.52	7.45	8.19	8.05	7.35	6.30	5.90	5.70	4.40

quoted E_0 values in our DDCSs are an average of these measurements.

Unfortunately, using the polynomial series in E of order $\leqslant 2$ to extrapolate the instrumental transmission determined for the He ionization continuum into the He ($n=2$) energy-loss region, a region inaccessible to our calibration techniques, resulted in a systematic error. To compensate for this error, the (relative) DDCSs were extrapolated to $\theta=0°$ and 180° and integrated over θ to obtain singly differential cross sections (SCDSs) or $d\sigma/dE(E_0,E)$. These SDCSs were then multiplied by factor 1/2 (to account for the scattered electron only) and integrated over E to obtain the total ionization cross section. This enabled us to normalize our results to the well-established and accurate (±3% uncertainties) total ionization cross sections measured by Shah *et al.* [26]. In the determination of our SDCSs, we extrapolated our DDCSs to small and large scattering angles using the form of the CCC. The error in this extrapolation was estimated by repeating the integration, but instead employing flat DDCS extrapolations to $\theta=0°$ and 180° from the end points of the angular distribution of the DDCSs. The error estimate was determined from the difference of the two extrapolations and added in quadrature with the mean error of our DDCSs.

B. Theory

The details of the application of the CCC theory to calculating differential e-He ionization cross sections have been recently discussed by Bray *et al.* [28] and Stelbovics *et al.* [22]. Briefly, the total electron-He wave function is expanded using a set of square-integrable target states with the resulting coupled integral equations solved in momentum space. The target states may be obtained using Laguerre- or box-based one-electron orbitals. These orbitals are used to define a configuration-interaction (CI) expansion. For dominant one-electron transitions, we find that the CI expansions need not include two-electron excitations, and so we may restrict one of the He electrons to remain in the 1s orbital of the He$^+$ ion while maintaining the required symmetries. Ionization amplitudes in the CCC theory are obtained directly from excitation amplitudes of the positive-energy target states [11]. The numerical parameters used in the present calculations are much the same as used earlier [28], except they were performed at the kinematics of the present experiment.

III. RESULTS

A. DDCS values

Table II gives the results of our measurements of the helium DDCSs, with uncertainties including the reproducibility of the continuum height (one standard deviation, $\approx$10–30%), a 12% uncertainty in the normalization to the He ($n=2$) experimental DCSs, and a relative transmission uncertainty of 10%. Of these, the reproducibility uncertainty was the most significant and was affected most by experimental instabilities, especially at small θ where very small variations in the electron beam geometry can result in significant changes in secondary electron backgrounds, in turn causing variations in the subtracted spectrum deduced from our moveable source setup. As the incident energy was increased, the reproducibility of the measurements was found to improve, which yielded smaller error bars.

Figures 2–8 illustrate our DDCSs compared to the existing low-energy measurements of Pichou *et al.* [23] and Röder *et al.* [24]. The DDCSs of Pichou *et al.* were taken from their published graphs. At E_0=26.3 eV (see Fig. 2), 1.7 eV above threshold, we compare our DDCSs at this E_0

TABLE II. (a) Present DDCSs for electron-impact ionization of helium and associated uncertainties (one standard deviation) for E_0=26.3 eV. Units are in 10^{-19} cm^2 sr^{-1} eV^{-1}. (b) Same as (a) but for E_0=28.3 eV. (c) Same as (a) but for E_0=30.3 eV. (d) Same as (a) but for E_0=32.5 eV. (e) Same as (a) but for E_0=34.3 eV. (f) Same as (a) but for E_0=36.5 eV. (g) Same as (a) but for E_0=40.7 eV.

(a)

E_R (eV) →	1.4		1.25		0.85		0.5		0.3	
θ (deg) ↓	DDCS	Error	DDCS	Error	DDCS	Error	DDCS	Error	DDCS	
10	3.52	0.78	3.79	1.40	3.07	0.66	4.37	1.21	3.16	0.95
20	3.47	0.78	3.14	0.89	3.21	0.81	4.43	1.24	2.78	0.90
30	2.47	0.47	2.81	0.89	2.51	0.65	3.30	0.97	2.65	0.85
40	1.64	0.41	1.66	0.43	1.70	0.51	1.72	0.44	1.73	0.43
50	1.10	0.30	1.15	0.29	1.23	0.36	1.28	0.35	1.32	0.31
60	1.09	0.43	1.05	0.28	1.04	0.30	1.03	0.28	1.02	0.26
70	1.69	0.41	1.68	0.45	1.66	0.52	1.65	0.42	1.65	0.41
80	1.81	0.55	1.84	0.26	1.84	0.30	1.87	0.36	1.91	0.43
90	2.20	0.55	2.42	0.76	2.39	0.45	2.37	0.69	2.36	0.57
100	1.61	0.48	1.58	0.46	1.53	0.45	1.50	0.45	1.48	0.40
110	1.91	0.60	1.87	0.53	1.80	0.43	1.76	0.37	1.73	0.33
120	1.47	0.33	1.44	0.30	1.39	0.27	1.36	0.26	1.33	0.27
130	1.67	0.26	1.59	0.26	1.45	0.29	1.36	0.32	1.30	0.34

(b)

E_R (eV) →	3.4		3.0		2.4		1.8		1.2		0.6	
θ (deg) ↓	DDCS	Error	DDCS	Error	DDCS	Error	DDCS	Error	DDCS	Error	DDCS	Error
10	8.93	1.55	8.23	1.77	7.21	1.32	6.17	1.33	5.03	1.21	3.73	1.28
20	5.05	1.35	4.87	1.24	4.58	1.14	4.28	1.12	3.93	1.19	3.18	1.01
25	4.31	0.90	4.16	0.96	3.97	1.07	3.80	0.87	3.64	1.07	2.83	0.66
30	3.41	0.96	3.29	0.94	3.12	0.93	2.91	0.92	2.66	0.95	2.33	0.83
40	1.86	0.47	1.88	0.48	1.92	0.55	1.96	0.69	2.02	0.81	1.61	0.58
50	1.23	0.41	1.22	0.31	1.20	0.40	1.18	0.40	1.15	0.41	1.10	0.42
60	1.46	0.40	1.46	0.39	1.46	0.39	1.46	0.39	1.46	0.42	1.47	0.49
70	1.66	0.41	1.64	0.41	1.60	0.40	1.56	0.45	1.50	0.52	1.40	0.56
80	1.49	0.27	1.44	0.28	1.35	0.31	1.25	0.35	1.13	0.40	0.95	0.37
90	1.76	0.41	1.76	0.42	1.76	0.43	1.77	0.46	1.76	0.51	1.76	0.60
100	1.47	0.34	1.44	0.34	1.38	0.36	1.31	0.38	1.21	0.43	1.05	0.52
110	1.70	0.36	1.69	0.37	1.66	0.37	1.62	0.39	1.56	0.42	1.47	0.49

TABLE II. (*Continued.*)

120	1.62	0.35	1.58	0.35	1.51	0.35	1.43	0.37	1.32	0.42	1.17	0.41
130	1.85	0.39	1.79	0.42	1.70	0.48	1.59	0.47	1.46	0.57	1.28	0.48

(c)

E_R (eV) →	5.4		4.5		3.5		2.5		1.5		1.0		0.5	
θ (deg) ↓	DDCS	Error	DDCS	Error	DDCS	Error	DDCS	Error	DDCS	Error	DDCS	Error	DDCS	Error
10	7.71	0.97	5.86	0.75	4.51	0.65	3.58	0.63	2.89	0.64	2.87	0.50	3.07	0.88
20	5.44	0.84	4.40	0.60	3.64	0.63	2.90	0.50	2.70	0.70	1.84	0.46	3.04	0.84
25	4.30	0.61	3.39	0.48	2.72	0.42	2.26	0.39	1.92	0.39	1.79	0.39	2.16	0.51
30	3.21	0.49	2.65	0.39	2.24	0.42	1.95	0.46	1.70	0.47	1.58	0.45	1.85	0.57
35	2.46	0.33	2.04	0.31	1.74	0.34	1.53	0.37	1.38	0.35	1.31	0.42	1.64	0.45
40	2.06	0.29	1.87	0.32	1.74	0.35	1.50	0.32	1.58	0.42	1.38	0.34	1.99	0.56
50	1.48	0.19	1.36	0.19	1.27	0.20	1.19	0.21	1.12	0.22	1.07	0.24	1.28	0.43
60	1.27	0.17	1.21	0.18	1.16	0.18	1.13	0.19	1.10	0.19	1.09	0.18	1.39	0.22
70	1.22	0.16	1.20	0.16	1.18	0.16	1.17	0.17	1.16	0.17	1.16	0.17	1.49	0.21
80	1.45	0.19	1.45	0.21	1.46	0.23	1.48	0.26	1.52	0.28	1.56	0.32	2.12	0.50
90	1.57	0.21	1.56	0.23	1.55	0.24	1.54	0.25	1.53	0.25	1.51	0.26	1.93	0.34
100	1.63	0.27	1.61	0.29	1.60	0.30	1.59	0.32	1.58	0.33	1.57	0.33	2.03	0.44
110	1.79	0.27	1.72	0.25	1.68	0.25	1.66	0.26	1.66	0.29	1.67	0.32	2.21	0.49
120	1.72	0.23	1.60	0.24	1.50	0.25	1.42	0.24	1.33	0.20	1.27	0.18	1.51	0.33
125	1.81	0.26	1.64	0.25	1.53	0.25	1.45	0.25	1.39	0.25	1.37	0.25	1.75	0.32
130	2.07	0.34	2.03	0.33	1.96	0.32	1.84	0.30	1.58	0.26	1.33	0.22	1.06	0.17

(d)

E_R (eV) →	7.4		6.5		5.5		4.5		3.5		2.5		1.5		0.5	
θ (deg) ↓	DDCS	Error	DDCS	Error	DDCS	Error	DDCS	Error	DDCS	Error	DDCS	Error	DDCS	Error	DDCS	Error
10	8.5	1.2	8.0	1.2	7.21	1.05	6.33	0.88	5.64	0.76	5.14	0.65	4.82	0.60	4.64	0.63
20	6.04	0.86	5.79	0.92	5.32	0.87	4.73	0.72	4.20	0.63	3.80	0.69	3.55	0.84	3.41	0.81
25	4.79	0.76	4.86	0.76	4.61	0.77	4.12	0.73	3.60	0.81	3.15	0.77	2.82	0.88	2.59	0.74
30	3.20	0.43	3.14	0.46	3.00	0.44	2.84	0.39	2.67	0.37	2.52	0.41	2.41	0.47	2.33	0.55
35	2.52	0.46	2.63	0.49	2.63	0.53	2.52	0.56	2.35	0.59	2.17	0.61	2.00	0.55	1.86	0.63
40	1.77	0.27	1.82	0.25	1.83	0.27	1.81	0.33	1.77	0.42	1.72	0.52	1.69	0.46	1.67	0.52
50	1.39	0.28	1.37	0.22	1.34	0.20	1.30	0.22	1.33	0.16	1.33	0.16	1.34	0.18	1.36	0.23
60	1.24	0.21	1.24	0.21	1.24	0.22	1.24	0.23	1.25	0.24	1.25	0.23	1.26	0.23	1.27	0.23

TABLE II. (*Continued.*)

70	1.23	0.22	1.19	0.15	1.21	0.15	1.28	0.19	1.38	0.28	1.48	0.36	1.26	0.31	1.07	0.18
80	1.25	0.19	1.38	0.19	1.47	0.20	1.49	0.21	1.44	0.21	1.38	0.21	1.31	0.22	1.26	0.22
90	1.27	0.27	1.31	0.24	1.36	0.27	1.40	0.27	1.36	0.23	1.34	0.26	1.31	0.28	1.29	0.30
100	1.31	0.16	1.48	0.18	1.59	0.21	1.59	0.21	1.52	0.20	1.42	0.19	1.32	0.17	1.24	0.16
110	1.27	0.15	1.45	0.17	1.54	0.19	1.52	0.18	1.42	0.17	1.29	0.16	1.17	0.15	1.07	0.13
120	1.49	0.18	1.66	0.21	1.75	0.24	1.71	0.24	1.60	0.23	1.46	0.21	1.34	0.19	1.24	0.17
125	1.38	0.18	1.59	0.20	1.72	0.21	1.69	0.21	1.57	0.20	1.42	0.18	1.28	0.16	1.16	0.15

(e)

E_R (eV) →	9.4		8.0		6.5		5.0		4.0		3.0		2.0		1.0	
θ (deg) ↓	DDCS	Error	DDCS	Error	DDCS	Error	DDCS	Error	DDCS	Error	DDCS	Error	DDCS	Error	DDCS	Error
10	12.3	1.7	9.0	1.2	7.2	1.0	5.77	0.80	5.13	0.77	4.55	0.66	4.33	0.64	4.11	0.53
20	7.28	0.96	5.78	0.81	4.93	0.69	4.09	0.53	3.63	0.46	3.29	0.43	3.06	0.46	2.91	0.50
25	5.41	0.70	4.39	0.66	3.89	0.62	3.37	0.49	3.09	0.42	2.89	0.41	2.75	0.48	2.68	0.55
30	3.92	0.57	3.28	0.50	3.04	0.46	2.78	0.41	2.64	0.38	2.53	0.37	2.45	0.39	2.40	0.41
35	3.10	0.40	2.60	0.32	2.47	0.31	2.35	0.30	2.29	0.30	2.26	0.31	2.24	0.33	2.24	0.34
40	2.32	0.46	2.00	0.35	1.98	0.29	1.96	0.26	1.96	0.26	1.96	0.27	1.96	0.28	1.97	0.29
50	1.33	0.16	1.11	0.14	1.13	0.14	1.20	0.16	1.25	0.17	1.31	0.18	1.36	0.20	1.19	0.18
60	1.24	0.16	1.12	0.14	1.13	0.14	1.12	0.14	1.10	0.14	1.09	0.14	1.07	0.15	1.06	0.15
70	1.10	0.14	0.99	0.12	1.02	0.12	1.05	0.13	1.07	0.13	1.08	0.14	1.09	0.15	1.10	0.15
80	1.13	0.14	1.06	0.13	1.11	0.14	1.12	0.14	1.11	0.14	1.09	0.14	1.07	0.13	1.04	0.13
90	1.16	0.20	1.05	0.18	1.09	0.20	1.12	0.21	1.14	0.22	1.15	0.22	1.16	0.20	1.16	0.23
100	1.27	0.16	1.18	0.15	1.24	0.16	1.26	0.17	1.26	0.17	1.26	0.18	1.25	0.19	1.24	0.19
110	1.38	0.19	1.33	0.21	1.42	0.24	1.43	0.25	1.41	0.25	1.37	0.25	1.34	0.25	1.30	0.24
120	1.41	0.17	1.38	0.20	1.49	0.26	1.53	0.26	1.53	0.23	1.51	0.21	1.48	0.20	1.45	0.20
125	1.55	0.21	1.28	0.15	1.33	0.16	1.49	0.19	1.61	0.23	1.73	0.28	1.84	0.33	1.94	0.36

(f)

E_R (eV) →	11.4		10.0		9.0		8.0		7.0		6.0		5.0		4.0		3.0		2.0		1.0	
θ (deg) ↓	DDCS	Error	DDCS	Error	DDCS	Error	DDCS	Error	DDCS	Error	DDCS	Error	DDCS	Error	DDCS	Error	DDCS	Error	DDCS	Error	DDCS	Error
10	13.89	1.85	12.07	1.60	10.62	1.43	9.14	1.30	7.73	1.22	6.47	1.20	5.43	1.24	4.46	1.10	4.11	0.88	3.53	0.80	3.37	0.86
20	7.64	1.04	6.92	0.98	6.33	0.94	5.71	0.89	5.11	0.85	4.56	0.81	4.09	0.77	3.71	0.75	3.44	0.74	3.26	0.74	3.17	0.75
25	5.54	0.82	5.07	0.74	4.70	0.68	4.31	0.62	3.94	0.58	3.61	0.55	3.34	0.54	3.13	0.54	2.98	0.56	2.90	0.59	2.87	0.63
30	3.91	0.55	3.73	0.56	3.56	0.57	3.38	0.59	3.19	0.62	3.01	0.66	2.85	0.74	2.68	0.54	2.39	0.66	2.82	0.71	2.60	0.33

TABLE II. (*Continued.*)

35	2.76	0.33	2.65	0.33	2.54	0.34	2.42	0.34	2.30	0.35	2.17	0.36	2.05	0.37	1.95	0.38	1.87	0.39	1.80	0.40	1.76	0.41
40	2.18	0.30	2.09	0.28	2.04	0.27	2.02	0.26	2.02	0.29	2.06	0.39	2.12	0.56	1.89	0.35	1.88	0.39	1.87	0.51	1.88	0.44
50	1.57	0.21	1.53	0.18	1.51	0.18	1.51	0.19	1.52	0.19	1.54	0.20	1.58	0.23	1.63	0.29	1.68	0.36	1.73	0.44	1.79	0.47
60	1.13	0.14	1.16	0.16	1.17	0.17	1.17	0.19	1.15	0.20	1.13	0.20	1.10	0.20	1.07	0.20	1.04	0.20	1.00	0.19	0.97	0.18
70	0.97	0.12	0.97	0.12	0.97	0.12	0.97	0.12	0.97	0.12	1.00	0.13	1.01	0.15	1.03	0.17	1.05	0.20	1.07	0.23	1.09	0.26
80	0.97	0.13	1.04	0.14	1.08	0.16	1.12	0.17	1.13	0.18	1.14	0.19	1.13	0.20	1.11	0.20	1.09	0.21	1.06	0.22	1.03	0.23
90	1.03	0.16	1.06	0.16	1.08	0.16	1.10	0.17	1.12	0.17	1.14	0.18	1.15	0.18	1.16	0.20	1.17	0.21	1.18	0.24	1.18	0.26
100	1.09	0.14	1.12	0.14	1.15	0.15	1.17	0.15	1.18	0.15	1.20	0.15	1.20	0.15	1.20	0.16	1.20	0.17	1.20	0.20	1.19	0.23
110	1.24	0.23	1.30	0.28	1.34	0.31	1.38	0.34	1.40	0.36	1.43	0.37	1.44	0.37	1.45	0.36	1.45	0.34	1.44	0.32	1.43	0.29
120	1.12	0.15	1.20	0.16	1.26	0.16	1.30	0.17	1.32	0.18	1.33	0.19	1.32	0.20	1.30	0.21	1.27	0.23	1.23	0.26	1.19	0.28
125	1.33	0.18	1.43	0.19	1.51	0.22	1.59	0.26	1.66	0.30	1.72	0.34	1.76	0.37	1.80	0.41	1.83	0.43	1.84	0.45	1.85	0.47

(g)

E_R (eV) →	15.0		14.5		13.0		11.5		10.0		8.5		7.0		5.5		4.0		2.5		1.0	
θ (deg) ↓	DDCS	Error	DDCS	Error	DDCS	Error	DDCS	Error	DDCS	Error	DDCS	Error	DDCS	Error	DDCS	Error	DDCS	Error	DDCS	Error	DDCS	Error
10	16.68	2.08	15.84	2.00	13.56	1.71	11.18	1.41	8.89	1.13	6.88	0.89	5.32	0.69	4.29	0.56	3.77	0.52	3.72	0.55	4.02	0.65
20	7.95	1.11	7.72	1.10	6.93	1.04	6.07	0.96	5.20	0.87	4.38	0.75	3.69	0.63	3.16	0.50	2.81	0.39	2.63	0.33	2.59	0.33
25	5.31	0.81	5.00	0.63	4.57	0.57	4.09	0.53	3.62	0.49	3.18	0.46	2.82	0.43	2.56	0.40	2.39	0.38	2.32	0.38	2.33	0.42
30	3.83	0.54	3.69	0.48	3.48	0.46	3.24	0.45	2.97	0.44	2.71	0.42	2.48	0.41	2.29	0.40	2.14	0.39	2.05	0.38	1.99	0.39
35	2.56	0.32	2.53	0.31	2.42	0.30	2.29	0.29	2.16	0.28	2.02	0.26	1.90	0.25	1.80	0.23	1.73	0.22	1.69	0.22	1.67	0.21
40	2.11	0.34	2.02	0.30	1.96	0.29	1.89	0.30	1.81	0.31	1.74	0.32	1.67	0.34	1.61	0.32	1.57	0.34	1.54	0.37	1.53	0.40
50	1.29	0.16	1.29	0.16	1.28	0.16	1.26	0.16	1.25	0.16	1.24	0.16	1.24	0.15	1.24	0.15	1.24	0.15	1.25	0.15	1.26	0.16
60	1.10	0.18	1.05	0.14	1.05	0.14	1.06	0.15	1.07	0.17	1.08	0.18	1.09	0.19	1.10	0.19	1.12	0.19	1.13	0.19	1.15	0.19
70	0.93	0.13	0.94	0.14	0.97	0.16	1.00	0.19	1.02	0.21	1.05	0.23	1.07	0.24	1.09	0.24	1.10	0.24	1.11	0.23	1.12	0.22
80	0.86	0.11	0.86	0.11	0.87	0.11	0.89	0.12	0.90	0.12	0.92	0.13	0.93	0.14	0.95	0.15	0.96	0.16	0.97	0.316	0.98	0.17
90	0.91	0.12	0.92	0.12	0.94	0.13	0.97	0.14	0.99	0.15	1.01	0.16	1.03	0.17	1.05	0.17	1.06	0.18	1.08	0.18	1.08	0.18
100	0.95	0.15	0.96	0.15	1.00	0.16	1.04	0.18	1.08	0.21	1.11	0.23	1.14	0.25	1.15	0.27	1.16	0.28	1.16	0.29	1.16	0.30
110	0.96	0.14	0.98	0.14	1.03	0.16	1.09	0.19	1.13	0.22	1.17	0.25	1.20	0.27	1.22	0.29	1.22	0.30	1.22	0.31	1.21	0.32
120	1.02	0.13	1.03	0.14	1.08	0.16	1.14	0.19	1.20	0.22	1.26	0.26	1.32	0.30	1.37	0.33	1.42	0.35	1.45	0.37	1.48	0.38
125	1.05	0.13	1.07	0.14	1.15	0.17	1.24	0.21	1.34	0.26	1.44	0.31	1.53	0.35	1.61	0.38	1.67	0.41	1.72	0.42	1.76	0.43

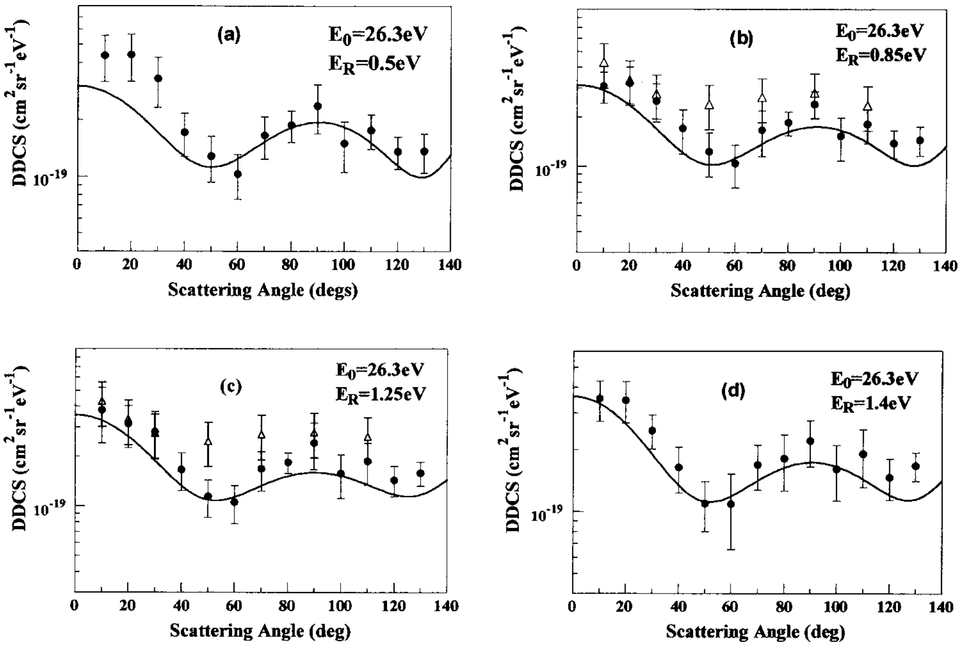

FIG. 2. Doubly differential cross sections for the electron-impact ionization of helium for $E_0 \approx 26.3$ eV. Legend: ●, present work at E_0=26.3 eV; △, Pichou *et al.* [23] at E_0=26.0 eV; and —, CCC at E_0=26.0 eV. (a) E_R=0.5 eV present; E_R=0.5 eV CCC. (b) E_R=0.85 eV present; E_R=0.7 eV Pichou *et al.*; E_R=0.85 eV CCC. (c) E_R=1.25 eV present; E_R=1.26 eV Pichou *et al.*; E_R=1.25 eV CCC. (d) E_R=1.4 eV present; E_R=1.4 eV CCC.

and E_R of 0.85 and 1.25 eV with the results of Pichou *et al.* [23] taken at the lower E_0 value of 26.0 eV and E_R of 0.7 and 1.26 eV, respectively, in Figs. 2(b) and 2(c). Although the Pichou *et al.* measurements are at a lower E_0 value than ours, their DDCSs exceed ours by as much as a factor of 2.5 at intermediate θ values. At small θ for E_R=1.25 eV, their DDCSs and ours are in excellent quantitative agreement, but disagree at larger θ. The overall quantitative disagreement could be due to their inability to correct properly for their secondary electron background, or to their normalization to the elastic DCSs, since the elastic feature is a large energy-loss interval from the ionization continuum feature in energy-loss spectra. The shapes of the two measurements are also in some disagreement. We note the lower uncertainties of the present work when compared to those of Pichou *et al.* [23]. Agreement with CCC is very good.

In Fig. 3 (around E_0=28.3 eV) the angular distributions of the present data and those of the CCC theory, Röder *et al.* [24], and Pichou *et al.* [23] are all in reasonable agreement. The angular distributions of Röder *et al.* [24] are taken over a much finer scale and show very good qualitative agreement with CCC, however they are much higher than CCC and the present results but lower than Pichou *et al.* [23], which are about three times larger than the present results over the entire angular range. The present results are in very good quantitative agreement with CCC for all E_R values at this E_0, except at small θ. The present results show somewhat improved agreement with Röder *et al.*'s DDCSs with increasing E_R. However, the structure displayed in the CCC and Röder *et al.*'s [24] DDCSs is not shown as clearly in our results.

At the E_0 value of 30.3 eV (Fig. 4), we see excellent qualitative agreement with the CCC at all E_R values, but

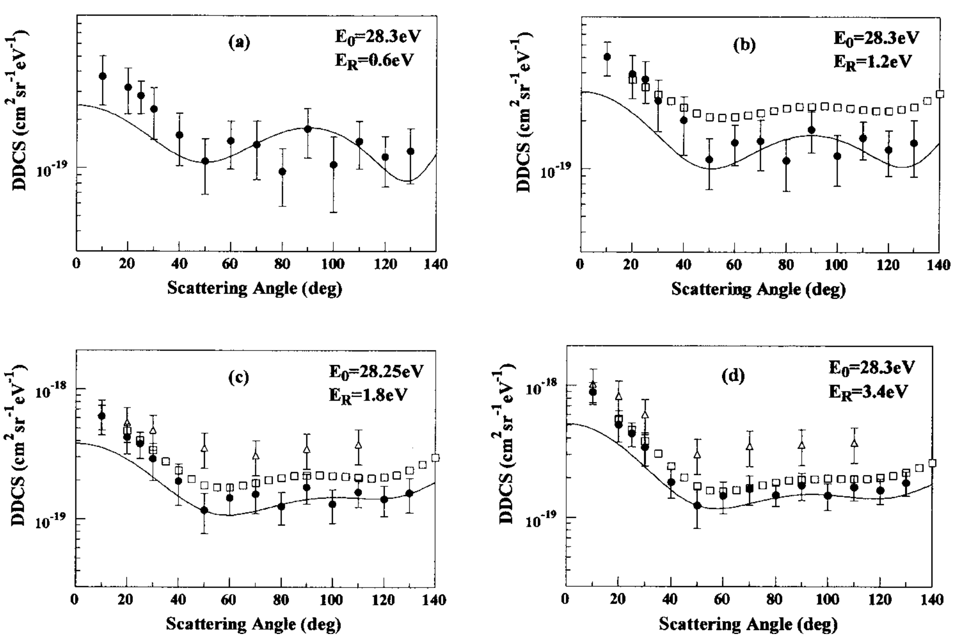

FIG. 3. Same as Fig. 2, but for the present work at E_0=28.3 eV; Pichou *et al.* at E_0=28.2 eV; CCC at E_0=28.0 eV. Additional legend: □, Röder *et al.* [24] at E_0=28.6 eV. (a) E_R=0.6 eV present; E_R=0.6 eV CCC. (b) E_R=1.2 eV present; E_R=1.2 eV Röder *et al.*; E_R=1.2 eV CCC. (c) E_R=1.8 eV present; E_R=1.8 eV Pichou *et al.*; E_R=1.8 eV Röder *et al.*; E_R=1.8 eV CCC. (d) E_R=3.4 eV present; E_R=3.24 eV Pichou *et al.*; E_R=3.0 eV Röder *et al.*; E_R=3.0 eV CCC.

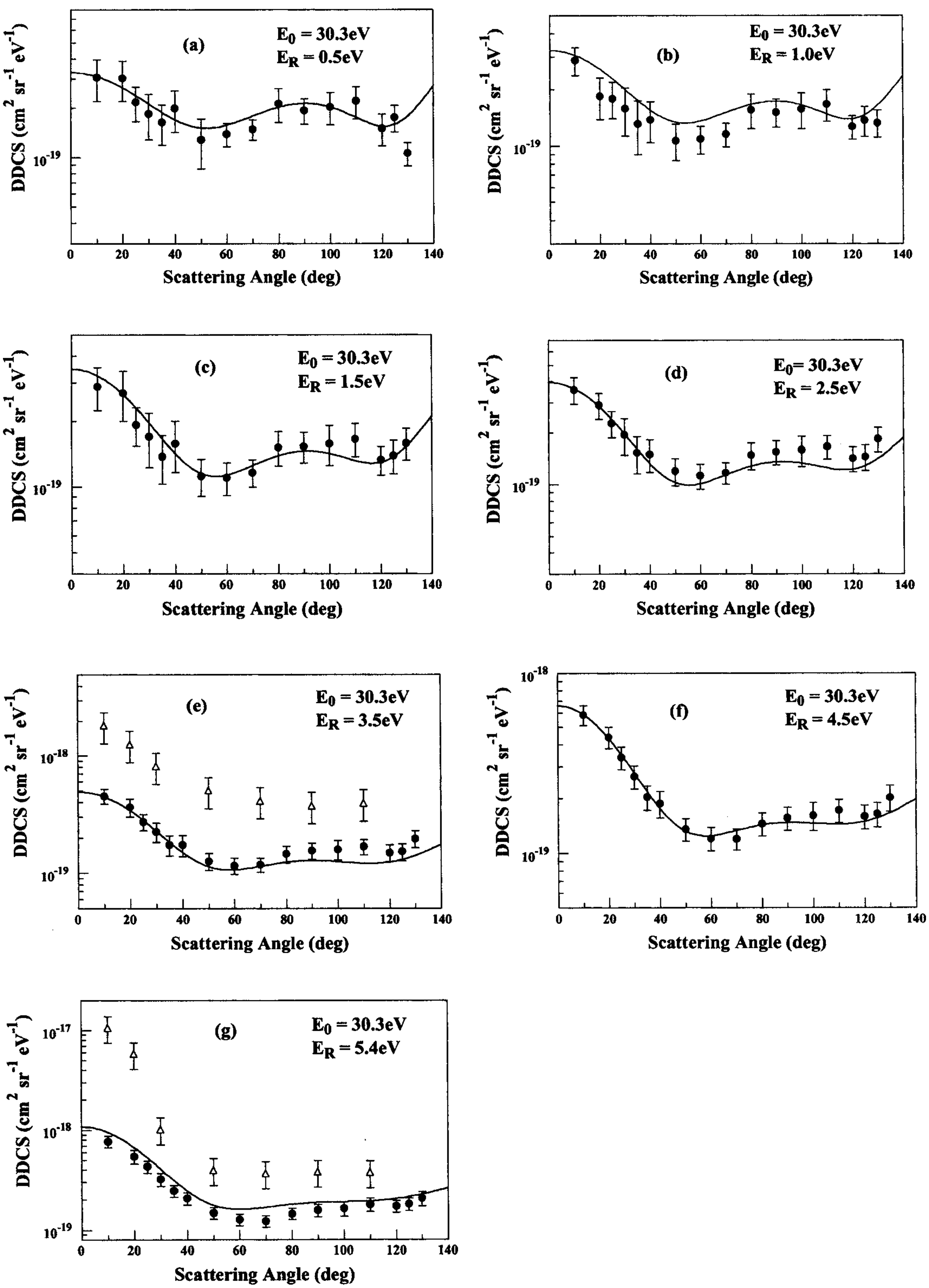

FIG. 4. Same as Fig. 3, but for the present work at E_0=30.3 eV; Pichou *et al.* at E_0=30.6 eV; CCC at E_0=30.0 eV. (a) E_R=0.5 eV present; E_R=0.5 eV CCC. (b) E_R=1.0 eV present; E_R=1.0 eV CCC. (c) E_R=1.5 eV present; E_R=1.5 eV CCC. (d) E_R=2.5 eV present; E_R=2.5 eV CCC. (e) E_R=3.5 eV present; E_R=3.0 eV Pichou *et al.*; E_R=3.5 eV CCC. (f) E_R=4.5 eV present; E_R=4.5 eV CCC. (g) E_R=5.4 eV present; E_R=5.4 eV Pichou *et al.*; E_R=5.4 eV CCC.

small (yet significant) differences in the magnitudes of the DDCSs. For example, at our highest E_R value [Fig. 4(g)] our DDCSs are generally lower than the CCC DDCSs by about 25%. Our results show disagreements with the results of Pichou *et al.* [23], who in some cases are a factor of >3 higher than our DDCSs. At the next higher E_0 value of 32.5 eV (Fig. 5) our DDCSs show overall excellent quantitative agreement with the CCC. However, our DDCSs are more

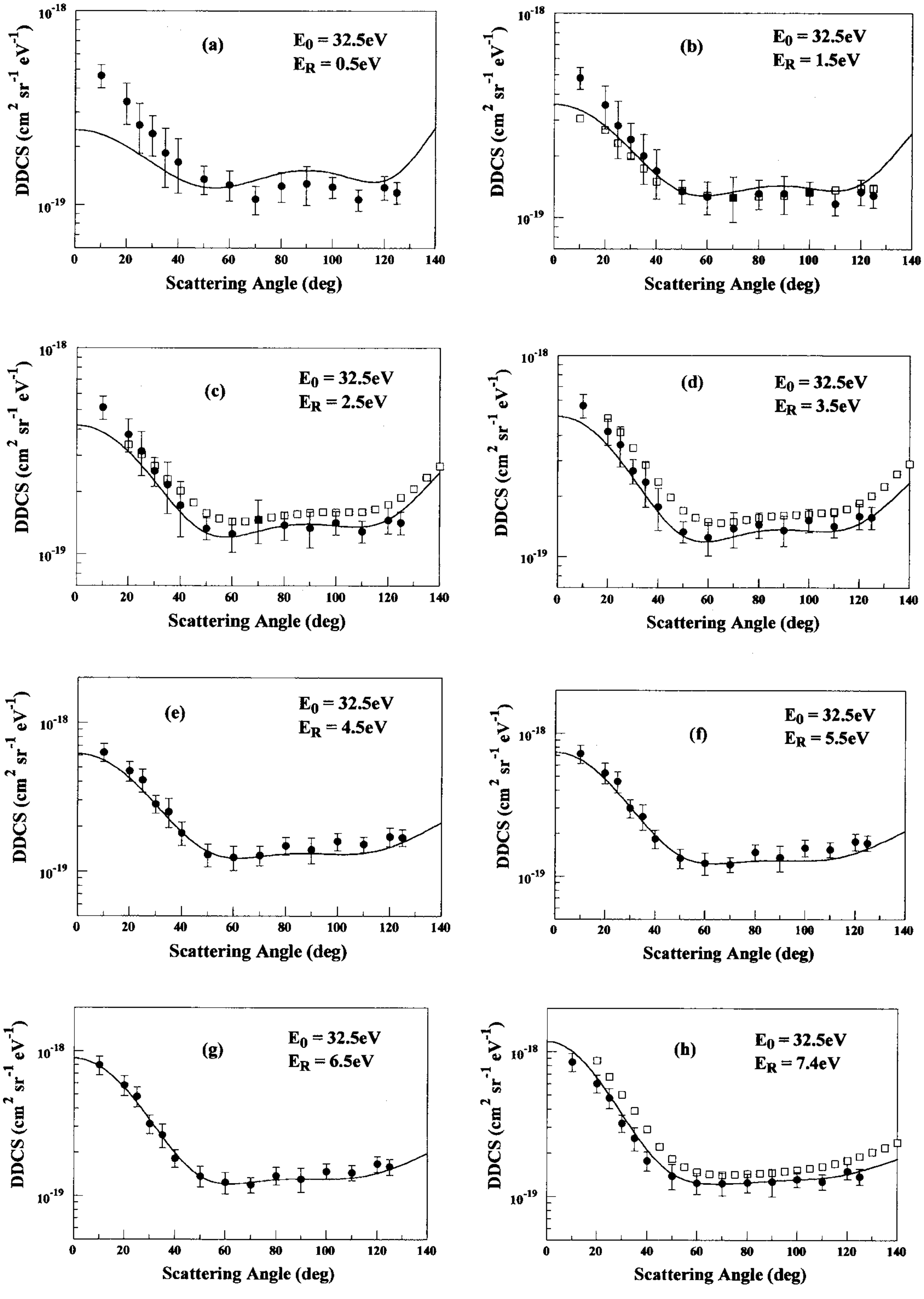

FIG. 5. Same as Fig. 3, but for the present work at E_0=32.5 eV; Röder *et al.* at E_0=32.6 eV; CCC at E_0=32.6 eV. (a) E_R=0.5 eV present; E_R=0.5 eV CCC. (b) E_R=1.5 eV present; E_R=2.0 eV Röder *et al.*; E_R=1.5 eV CCC. (c) E_R=2.5 eV present; E_R=2.5 eV Röder *et al.*; E_R=2.5 eV CCC. (d) E_R=3.5 eV present; E_R=3.5 eV Röder *et al.*; E_R=3.5 eV CCC. (e) E_R=4.5 eV present; E_R=4.5 eV CCC. (f) E_R=5.5 eV present; E_R=5.5 eV CCC. (g) E_R=6.5 eV present; E_R=6.5 eV CCC. (h) E_R=7.4 eV present; E_R=7.7 eV Röder *et al.*; E_R=7.5 eV CCC.

forward-peaked than CCC for small E_R values [Figs. 5(a) and 5(b)]. At the highest E_R value of 7.4 eV [Fig. 5(h)], excellent quantitative agreement with the CCC is observed, as well as excellent qualitative agreement with the Röder *et al.* DDCSs, as both now show a single minimum around θ=70°. We note especially small θ, for the low E_R value of 1.5 eV [Fig. 5(b)], where the Röder *et al.* [24] measurements (taken at a slightly higher E_R=2.0 eV) display a lower

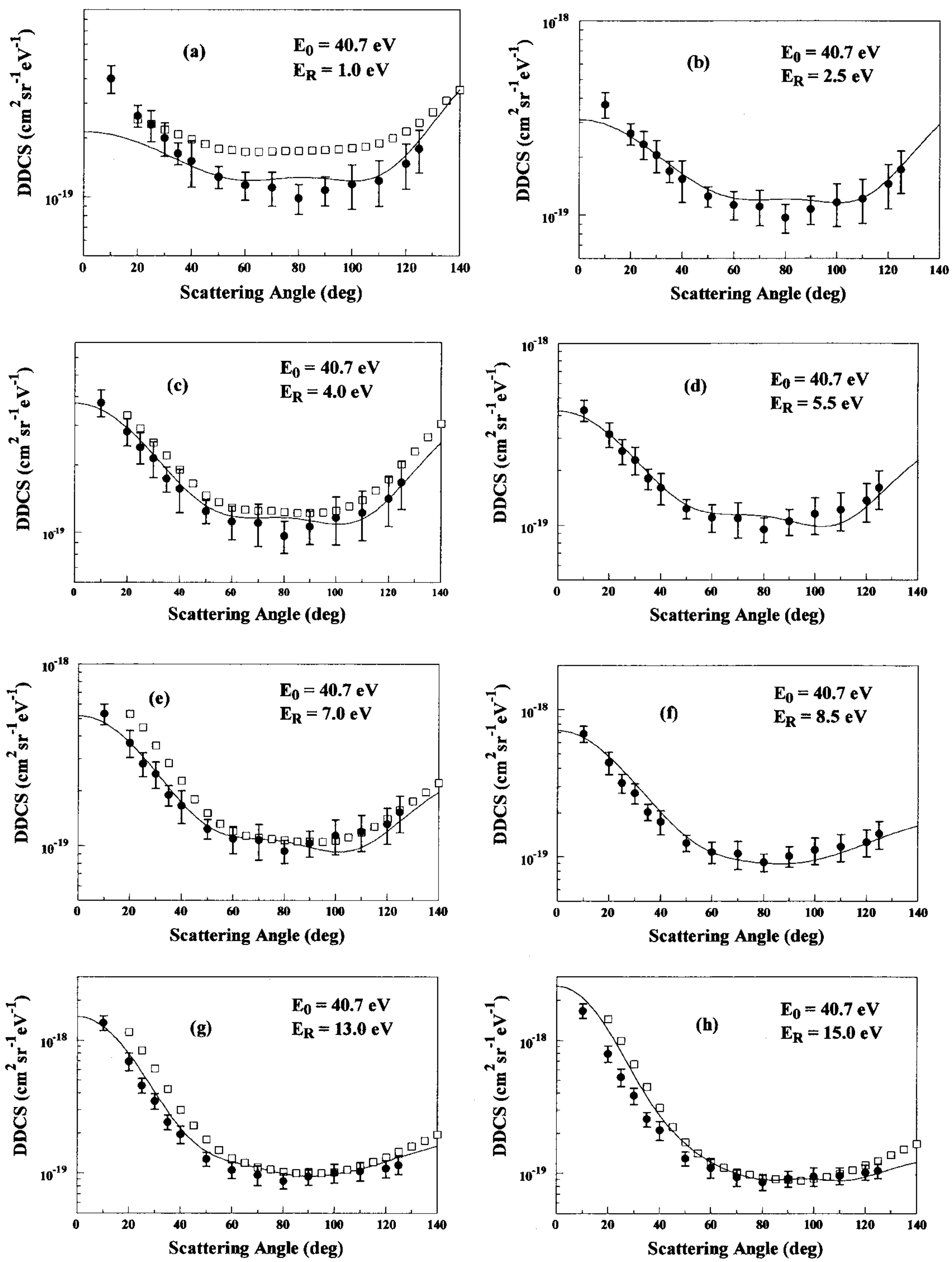

FIG. 6. Same as Figs. 2 and 3, but for the present work at E_0=40.7 eV; Röder *et al.* at E_0=40 eV; CCC at E_0=40 eV. (a) E_R=1.0 eV present; E_R=1.0 eV Röder *et al.*; E_R=0.5 eV CCC. (b) E_R=2.5 eV present; E_R=2.5 eV CCC. (c) E_R=4.0 eV present; E_R=3.8 eV Röder *et al.*; E_R=4.0 eV CCC. (d) E_R=5.5 eV present; E_R=5.5 eV CCC. (e) E_R=7.0 eV present; E_R=7.7 eV Röder *et al.*; E_R=7.0 eV CCC. (f) E_R=8.5 eV present; E_R=8.5 eV CCC. (g) E_R=13.0 eV present; E_R=12.7 eV Röder *et al.*; E_R=13.0 eV CCC. (h) E_R=15.0 eV present; E_R=15.7 eV Röder *et al.*; E_R=15.0 eV CCC.

DDCS than ours and show excellent agreement with CCC for all θ.

At the next higher E_0 values of 34.3 and 36.5 eV (not plotted here), we observe very good overall qualitative agreement with CCC at all E_R values. Quantitative agreement with CCC is excellent for larger E_R values and very good at lower E_R values.

At the highest E_0 value of 40.65 eV (Fig. 6) we see excellent agreement with the CCC DDCSs at most E_R values [Figs. 6(b)–6(g)] except at the lowest E_R of 1 eV, where our

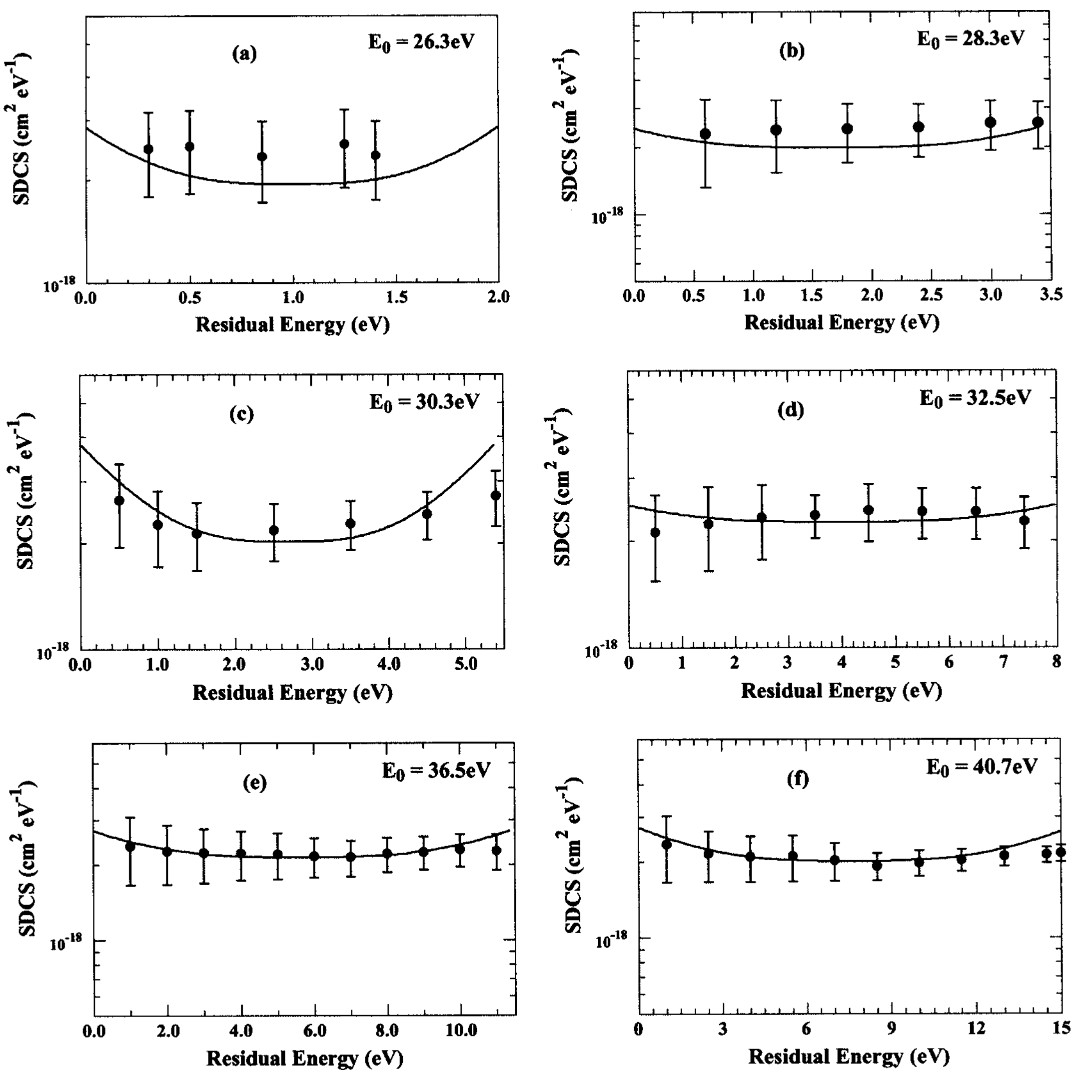

FIG. 7. Present normalized helium SDCSs. The present SDCSs were normalized to the total ionization cross sections of Shah *et al.* [26]. See text for details. (a) Legend: ●, present work at E_0=26.3 eV; —, CCC at E_0=26.0 eV. (b) Same as (a) but for the present work at E_0=28.3 eV and CCC at E_0=28.0 eV. (c) Same as (a) but for the present work at E_0=30.3 eV and CCC at E_0=30.0 eV. (d) Same as (a) but for the present work at E_0=32.5 eV and CCC at E_0=32.0 eV. (e) Same as (a) but for the present work at 36.5 eV and CCC at E_0=36.0 eV. (f) Same as (a) but for the present work at E_0=40.7 eV and CCC at E_0=40.0 eV.

DDCS shows a more pronounced forward peak than the CCC and the DDCS of Röder *et al.*, and the highest E_R of 15 eV, where our DDCS shows a smaller forward peak than either the CCC or the DDCS of Röder *et al.* The results of Röder *et al.* [24] show overall excellent qualitative agreement with the CCC, but at the lowest E_R of 1 eV they are in significant disagreement with both the CCC and our results.

Summarizing the DDCSs, we note the increasing backward peak of the angular distributions for the higher E_0 and lower E_R measurements. This effect confirms the well-known binary (or recoil) peak results for ionization. At large momentum transfer kinematics, the ionizing electron polarizes the atom, which effectively "pushes" the slower electron out to backward angles, while the fast electron emerges in the forward direction. The overall agreement with the CCC theory is very good in most cases and excellent in many. At low E_R values, our DDCS errors are unfortunately larger than at high E_R values, a situation that needs to be improved if we are to more stringently test theory at these low E_R values.

B. Singly differential cross-sections

Figures 7(a)–7(f) show our normalized SDCSs compared to the CCC calculations. As mentioned before, these experimental SDCSs were normalized to the total cross sections of Shah *et al.* [26]. In all cases, excellent agreement with CCC is observed, albeit within the large error bars of our SDCSs. We note that for all E_0 values, our SDCSs do not show the curved profiles displayed by CCC, but instead preferentially show a flat profile. We also note the increased uncertainties at small E_R due to uncertainties in the DDCS extrapolations during the integration of these data to yield SDCSs (see Sec. II for discussion).

C. Shape of DDCSs at θ=90°

The threshold ionization process has been treated theoretically in several different approaches. In the well-known

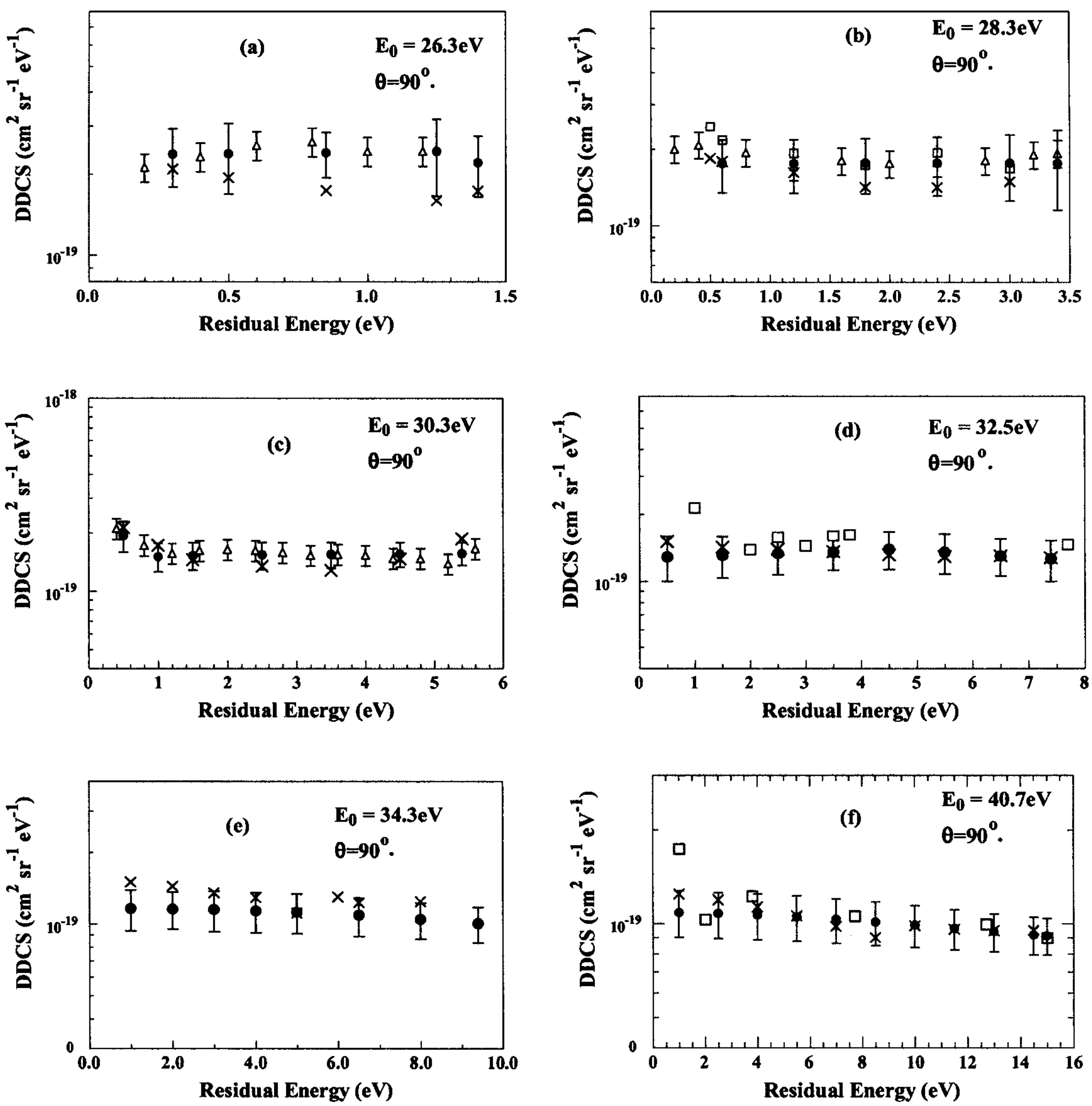

FIG. 8. Helium DDCSs for θ=90°. See text for discussion. (a) Legend: ●, present work at E_0=26.3 eV, △, Pichou *et al.* [23] at E_0=26.0 eV scaled down by 0.85;×, CCC at E_0=26.0 eV. (b) Same as (a) but for the present work at E_0=28.3 eV and Pichou *et al.* at E_0=28.2 eV scaled down by 0.5; □, Röder *et al.* [24] at E_0=28.0 eV and CCC at E_0=28.0 eV. (c) Same as (b) but for the present work at E_0=30.3 eV, Pichou *et al.* at E_0=30.7 eV scaled down by 0.38, and CCC at E_0=30.0 eV. (d) Same as (b) but for the present work at E_0=32.5 eV, Röder *et al.* at E_0=32.0 eV, and CCC at E_0=32.0 eV. (e) Same as (a) but for the present work at E_0=34.3 eV and CCC at E_0=34.0 eV. (f) Same as (b) but for the present work at E_0=40.7 eV and Röder *et al.* at E_0=40.0 eV and CCC at E_0=40.0 eV.

work of Wannier [49], which was later extended by Vinkalns and Gailitis [50], it is assumed that in the inner reaction zone the trajectories of the outgoing electrons fill the available phase space with a smooth and nonsingular probability; when outside this reaction zone, the electron trajectories are classical. One of the predictions of this theory including several quantum-mechanical models (see, e.g., Rau [51]) is that the kinetic energy distribution of the electrons is uniform. Detailed studies of the dynamics of the Wannier near-threshold behavior were performed by Cvejanović and Read [52]. They showed that at the E_0 value of 25.4 eV (0.8 eV above threshold), for the ionized electrons emitted coincidentally in directions of 90° and 270° from the incident electron direction, the energy partitioning between the two outgoing electrons was uniformly distributed within E_R. This was further investigated by Pichou *et al.* [23] using ad hoc background-corrected continua electron-energy-loss spectra with energies up to 6 eV above threshold. Their results showed a reasonably uniform distribution of ejected electron energy partitioning at θ=90° for E_0 up to 30.6 eV. This important observation by Pichou *et al.* has often been used to calibrate the transmission of electron spectrometers for scattered electrons (see Nickel *et al.* [42]). In Fig. 8, we show our DDCSs at 90° for all our E_0 values in this experiment and compare these to the results of the DDCSs of Pichou *et al.*, Röder *et al.* and CCC. We note here that the smoothness of our results is due to the averaging of the polynomial fits to our DDCS data, as discussed earlier.

We note several trends in the DDCSs. First, we are only able to reliably go to an E_R minimum of 0.5 eV at low E_0

values. Secondly, the DDCSs remain essentially flat up until E_0=32.5 eV within a deviation of 5%, and then progressively slope downward as a function of E_R at higher E_0 values. For example, at E_0=40.7 eV [Fig. 8(f)], the DDCSs drop by about 15% as E_R goes from 1.0 to 15.0 eV. This drop is almost linear. Agreement with the results of Pichou *et al.* and Röder *et al.* is mixed at low E_0 values below 30 eV, but improves as E_0 increases above this. In general, the shapes stay in very good agreement within the 15% error bars at low E_0, but improve to within 8% at 40 eV. The DDCS taken at E_0=40.7 eV significantly extends the use of the helium continuum and discrete energy-loss spectrum for spectrometer transmission calibrations to an E_R range of 1.0 eV up to approximately 20.0 eV ($1\,^1S \rightarrow 2\,^3S$ line), which is almost double the range at E_0=30.6 eV provided by Pichou *et al.* We note also that at E_0=30.3 eV, the results of CCC and Pichou *et al.* [23] show a significant increase ($\approx$50%) in the DDCS for $E_R < 1$; this is also suggested by our results, albeit with larger error bars. The Röder *et al.* data show this increase in all their 90° data. This feature needs to be investigated in detail in future studies.

IV. CONCLUSIONS

We have systematically determined quantitative DDCSs from background-corrected electron-He energy-loss spectra at energies from 1.7 eV above threshold to 16.1 eV above threshold. This was made possible by our moveable source method. Our results show very good quantitative agreement with the present CCC calculations and are expected to be an improvement over earlier measurements. In most cases, qualitative agreement with the DDCSs of Röder *et al.* [24] is very good, as is the agreement with the DDCSs of Pichou *et al.* [23], though not always quantitatively. At the highest E_0 and larger E_R we expect our DDCSs to suffer the least from systematic errors and to be a good place to test theoretical models. At small E_R, difficulties in quantitatively reproducing the He continuum spectrum, especially at small θ, due to larger secondary electron backgrounds lead to increased uncertainties in the results and prevent the present experiment from providing very precise data to test theory in this important range. This problem will be investigated in depth in future experiments.

ACKNOWLEDGMENTS

This work was funded by the National Science Foundation under the Research in an Undergraduate Institution NSF-RUI-PHY-9731890 and NSF-RUI-PHY-09354961. The authors thank Dr. Mark Baertschy for providing atomic hydrogen ECS DDCSs used in the calibration of the present experimental data. The authors also thank Hugo Fabris (electronics), David Parsons (machining), and Jorg Meyer (glass blowing). Additional help from Kenneth James, Jr. and Steve Mahrley is gratefully acknowledged. I.B. and D.V.F. are grateful for the support of the Australian Research Council, and ISA Technologies, Perth, Western Australia, for provision of access to their IBM P690 computer.

[1] D. F. Register, S. Trajmar, and S. K. Srivastava, Phys. Rev. A **21**, 1134 (1980).
[2] R. I. Hall, G. Joyez, J. Mazeau, J. Reinhardt, and C. Schermann, J. Phys. (Paris) **34**, 827 (1973).
[3] G. J. Schulz, Rev. Mod. Phys. **45**, 333 (1973).
[4] M. Eminyan, K. B. MacAdam, J. Slevin, and H. Kleinpoppen, Phys. Rev. Lett. **31**, 576 (1973).
[5] H. Ehrhardt, K. Jung, G. Knoth, and P. Schlemmer, Z. Phys. D: At., Mol. Clusters **1**, 3 (1986).
[6] D. V. Fursa and I. Bray, Phys. Rev. A **52**, 1279 (1995).
[7] I. Bray, D. V. Fursa, and I. E. McCarthy, J. Phys. B **27**, L421 (1994).
[8] D. V. Fursa and I. Bray, J. Phys. B **30**, 757 (1997).
[9] J. Röder, H. Ehrhardt, I. Bray, and D. V. Fursa, J. Phys. B **29**, L421 (1996).
[10] J. Röder, H. Ehrhardt, I. Bray, D. V. Fursa, and I. McCarthy, J. Phys. B **29**, L67 (1996).
[11] I. Bray and D. V. Fursa, Phys. Rev. A **54**, 2991 (1996).
[12] M. S. Pindzola, F. Robicheaux, J. P. Colgan, M. C. Witthoeft, and J. A. Ludlow, Phys. Rev. A **70**, 032705 (2004).
[13] D. A. Horner, C. W. McCurdy, and T. N. Rescigno, Phys. Rev. A **71**, 012701 (2005).
[14] J. G. Childers, K. E. James, Jr., I. Bray, M. Baertschy, and M. A. Khakoo, Phys. Rev. A **69**, 022709 (2004).
[15] K. Jung, R. Muller-Fiedler, P. Schlemmer, H. Ehrhardt, and H. Klar, J. Phys. B **18**, 2955 (1985).
[16] P. Schlemmer, M. K. Srivastava, T. Rosel, and H. Ehrhardt, J. Phys. B **24**, 2719 (1991).
[17] T. Rosel, J. Röder, L. Frost, K. Jung, H. Ehrhardt, S. Jones, and D. H. Madison, Phys. Rev. A **46**, 2539 (1992).
[18] T. Rosel, J. Röder, K. Jung, and H. Ehrhardt, J. Phys. B **25**, 3859 (1992).
[19] J. Röder, H. Ehrhardt, C. Pan, A. F. Starace, I. Bray, and D. V. Fursa, J. Phys. B **31**, L525 (1998).
[20] S. Jones, D. H. Madison, and M. K. Srivastava, J. Phys. B **25**, 1899 (1992).
[21] C. Pan and A. F. Starace, Phys. Rev. A **45**, 4588 (1992).
[22] A. T. Stelbovics, I. Bray, D. V. Fursa, and K. Bartschat, Phys. Rev. A **71**, 052716 (2005).
[23] F. Pichou, A. Huetz, G. Joyez, and M. Landau, J. Phys. B **11**, 3683 (1978).
[24] J. Röder, H. Ehrhardt, I. Bray, and D. V. Fursa, J. Phys. B **30**, 1309 (1997).
[25] D. Andrick and A. Bitsch, J. Phys. B **8**, 393 (1975).
[26] M. B. Shah, D. S. Elliot, P. McCallion, and H. B. Gilbody, J. Phys. B **21**, 2751 (1988).
[27] I. Bray and D. V. Fursa, Phys. Rev. Lett. **76**, 2674 (1996).
[28] I. Bray, D. V. Fursa, and A. T. Stelbovics, J. Phys. B **36**, 2211 (2003).
[29] C. B. Opal, E. C. Beaty, and W. K. Peterson, At. Data **4**, 209 (1972).
[30] N. Oda, Radiat. Res. **64**, 80 (1975).

[31] M. E. Rudd and R. D. DuBois, Phys. Rev. A **16**, 26 (1977).
[32] T. W. Shyn and W. E. Sharp, Phys. Rev. A **19**, 557 (1979).
[33] R. Müller-Fiedler, K. Jung, and H. Ehrhardt, J. Phys. B **19**, 1211 (1986).
[34] T. Rösel, P. Schlemmer, J. Röder, L. Frost, K. Jung, and H. Ehrhardt, J. Phys. B **29**, 2103 (1996).
[35] M. A. Khakoo P. Vandeventer, J. G. Childers, I. Kanik, C. J. Fontes, K. Bartschat, V. Zeman, D. H. Madison, S. Saxena, R. Srivastava, and A. D. Stauffer, J. Phys. B **37**, 247 (2003).
[36] M. A. Khakoo P. W. Johnson, I. Ozkay, P. Yan, S. Trajmar, and I. Kanik, Phys. Rev. A **71**, 062703 (2005).
[37] J. Childers, K. James, Jr., M. Hughes, I. Bray, M. Baertschy, and M. A. Khakoo, Phys. Rev. A **68**, 030702(R) (2003).
[38] J. G. Childers, K. E. James, Jr., Igor Bray, M. Baertschy, and M. A. Khakoo, Phys. Rev. A **69**, 022709 (2004).
[39] M. Hughes, K. E. James, Jr., J. G. Childers, and M. A. Khakoo, Meas. Sci. Technol. **15**, 841 (2003).
[40] M. Baertschy, T. N. Rescigno, W. A. Isaacs, X. Li, and C. W. McCurdy, Phys. Rev. A **63**, 022712 (2001).
[41] M. Baertschy (private communication).
[42] J. C. Nickel, P. W. Zetner, G. Shen, and S. Trajmar, J. Phys. E **22**, 730 (1989).
[43] F. Rugamas, D. Roundy, G. Mikaelian, G. Vitug, M. Rudner, J. Shih, D. Smith, J. Segura, and M. A. Khakoo, Meas. Sci. Technol. **11**, 1750 (2000).
[44] K. R. Asmis and M. Allan, J. Phys. B **30**, 1961 (1997).
[45] M. Larsen and M. A. Khakoo (unpublished).
[46] J. Röder, H. Ehrhardt, I. Bray, and D. V. Fursa, J. Phys. B **29**, L421 (1996).
[47] D. C. Cartwright, G. Csanak, S. Trajmar, and D. F. Register, Phys. Rev. A **45**, 1602 (1992).
[48] D. Cubric, D. J. L. Mercer, J. M. Channing, G. C. King, and F. H. Read, J. Phys. B **32**, L45 (1999).
[49] G. H. Wannier, Phys. Rev. **90**, 817 (1953).
[50] I. Vinkalns and M. Gailitis, *V ICPEAC* (Nauka, Leningrad, 1967), p. 648.
[51] A. R. P. Rau, Phys. Rev. A **4**, 207 (1971).
[52] S. Cvejanović and F. H. Read, J. Phys. B **14**, 1841 (1974).